ARCHIVES OF ELECTRICAL ENGINEERING VOL. 65(3), pp. 613-627 (2016)

DOI 10.1515/aee-2016-0044

Estimation of power losses in a high-frequency planar transformer using a thermal camera

ROMAN BARLIK, MIECZYSŁAW NOWAK, PIOTR GRZEJSZCZAK, MARIUSZ ZDANOWSKI

Institute of Control and Industrial Electronics, Warsaw University of Technology
Koszykowa 75, 00-662 Warszawa, Poland
e-mail: roman.barlik@ee.pw.edu.pl

(Received: 16.11.2015, revised: 21.03.2016)

Abstract: This paper presents the implementation of a thermal camera for the quantitative estimation of power losses in a high frequency planar transformer (100 kHz/ 5600 VA). The methodology is based on the observation of the transient temperature rise and determination of the power losses by means of curves representing the derivative of temperature as a function of power losses dissipated in the transformer. First, the thermal calibration characteristics had to be obtained from a simple experiment, where power losses are generated by DC current in the ferrite core and windings. Next, experimental investigations focused on the determination of the transformer power losses for a short circuit and no load, with a resistive load and with the rectifier as a load were carried out. Finally, to verify the obtained results, analytical calculations based on Dowell's and modified Steinmetz's equations were additionally made, which showed a good convergence. The proposed method is easy to implement and can be used as an alternative to the calorimetric method which is time-consuming and requires a complicated measurement setup.

Key words: power losses estimation, thermal camera, thermal calibration, planar transformer, Dowell's and Steinmetz's equations

1. Introduction

The estimation of the power losses of converter components such as semiconductor devices (transistors, diodes) or passive parts like transformers and inductors is described in a number of papers (e.g. [1-3]). This is a very important issue for improving the power density factor and power converter miniaturization. A detailed analysis of heat distribution from these components in high power density converters allows better thermal management and cooling conditions [4-6]. Many power electronics converters are characterized by a high switching frequency (f > 20 kHz) in the form of non-sinusoidal current and voltage waveforms, which makes the determination of the power losses more complicated.

There are various methods for power loss measurement, which are based on current and voltage scope records [2, 3]. However, they are characterized by low accuracy and have a few

measurement errors resulting from probe delays and large variations in voltage and current levels. It should be added that in the case of high-frequency converters the electromagnetic radiation reduces the accuracy of power measurements. Other relevant papers [7-9] analyze power losses in each part of the Dual Active Bridge converter (DAB), but the equations presented by the authors are complicated and thus difficult to use in practice. Very valuable information about the estimation of copper and core losses in transformers operated at a high frequency (above 20 kHz) is presented in reference [10]. There are also methods based on the analysis of thermal phenomena. For example, precise results can be achieved using a calorimetric method described in references [11-14], but the measurement process is time-consuming and requires a complex measurement setup. A significant time reduction in calorimetric measurements can be obtained by using the temperature rise analysis only [15, 16]. Finally, an ac-curate and simple method is presented in reference [17], though its application is limited to small converters with power losses of up to 30 W.

A method similar to the calorimetric method is discussed in this paper. It relies on the observation the transient temperature rise in the transformer and determination of the power losses using curves representing the derivative of the temperature as a function of power losses dissipated in the object being tested. In order to evaluate this method for the design of high frequency transformers, records of the surface temperature rise on the examined device must be taken. Additionally, a transformer supplied from an H-bridge converter was tested under several types of loads.

The authors assumed that with a good knowledge of the construction of the transformer, including the geometric arrangement of the coils, core material and dimensions, the power loss calculation results based on the Steinmetz and Dowell models were relatively accurate, [11] [18-21]. Hence to validate the results, the power losses measured in the core and windings were compared with the results of analytical calculations made using the modified Steinmetz equation for core losses and the Dowell equation for windings losses.

This paper is organized as follows: the measurement methodology and the experimental setup are described in Section 2. Detailed calculations of power losses for the transformer under laboratory testing are given in Section 3. Section 4 compares the results obtained from the thermal camera measurements with the analytical calculations using Steinmetz's and Dowell's formulas. Finally, conclusions are presented in Section 5.

2. Transformer loss measurements using a thermal camera

In order to examine the validity of the proposed method, a commercially available 5600 VA/100 kHz transformer was selected. The main parameters of this transformer are presented in Section 3. The proposed high-frequency transformer power loss measurement procedure consists of two steps. The first step involves the calibration of the measurement equipment by heating the main transformer components (core and windings) using a DC power supply, as the supplied power has to be precisely regulated. The second step is used to

estimate the power losses in the tested transformer under predefined loads using the heating curves obtained in the first step.

2.1. Experimental investigations

The principle of the calibration process relies on the recording the temperature as a function of time for several, known, constant values of the power dissipated in the transformer. First, the time-temperature curves for the different power losses of a planar transformer, which core and windings are heated by a separate DC power source are measured using an infrared camera, then the curves of power versus a temperature time derivative (dT_T/dt) are extracted for the power losses of the core and windings separately and together. Therefore, it is possible to determine the total power losses dissipated as heat both in the core and in the windings using a comparative method, if we know the relationship between the time derivative of the average transformer surface temperature and the overall power losses generated in the element being tested. To obtain this relationship, the precise DC power is delivered to the transformer and the averaged temperatures on the surface of this element are gathered. These thermal observations and measurements are used to provide calibration characteristics. The procedure for preparing such characteristics should be dedicated for each specific type of device, and could be described as a transformer "thermal calibration".

In the first step of the calibration process, the initial parts of the heating curves are determined by supplying the defined power to the ferrite core and the windings using a fully controlled DC voltage and the current sources as shown in Fig. 1a [11]. The thermal time constants of magnetic elements in small power electronic equipment vary from 10 to 20 minutes, but in practice, the transformer temperature T_T can be measured over a period of time not exceeding 10 minutes from the start of the calibration process. During calibration, the transformer should be placed in a protection case to minimize the measurement errors caused by external influences, such as air flow, draught, etc. For the temperature measurement, a thermal camera positioned above the tested transformer was used (Fig. 1b). The image obtained from the camera (Fig. 1c) shows the top surface of the transformer. The image is transferred to a PC where the average temperature of a predefined area was computed by dedicated software. The measurement area is marked out with the rectangle defined by the four cursors (Fig. 1c). The setup is detailed described by authors of this paper in [22]. It is worth noting that the majority of the thermal cameras currently available on the market have their own function of averaging the temperature over selected area.

During the calibration and testing under different transformer load conditions (as described in Section 3) camera must stay in the same position with respect to the transformer in order to capture the same surface emissivity.

The thermal calibration process was carried out in three cases – when power supply (equivalent of power losses P) was provided: a) only to the core, b) only to the windings, and c) both to the core and to the windings simultaneously (Fig. 1a). Power to the core was supplied by connecting a controlled DC voltage source directly to the ferrite core. To avoid high contact resistance, specially designed copper electrodes were used. Power to both windings was provided using two additional voltage sources (one for each winding).

The core heating power during the calibration process was determined as the product of voltage (*V*3) and current (*A*3). The resistance of the core varies with the core temperature and supplied voltage, so it is difficult to keep a constant power. The DC voltage had to be adjusted, taking into account this variable resistance.

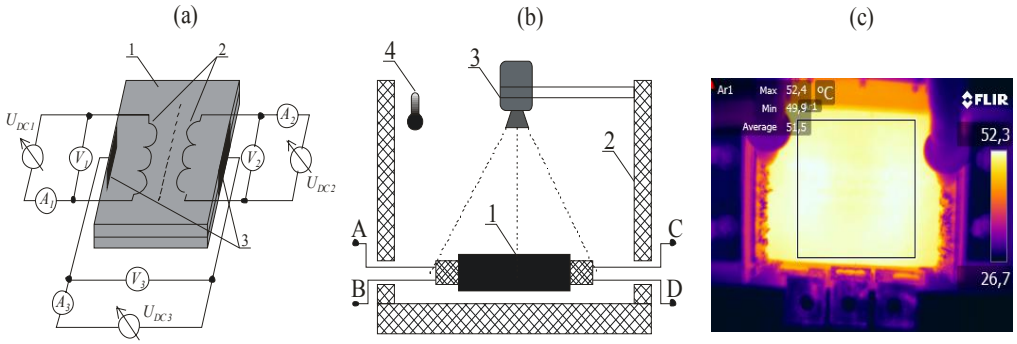

Fig. 1. Thermal testing of a transformer: (a) diagram of the transformer with the DC supply system: 1 – planar transformer, 2 – windings, 3 – copper electrodes; (b) view of the setup: 1 – tested element, 2 – protection case, 3 – thermal camera, 4 – thermometer to measure the temperature inside the case, A ÷ D – terminals of the transformer windings; (c) example of the camera image when the core is heated by DC current of 10 W after 15 min from the start of the test

In the second case, the DC voltages U_{DC1} and U_{DC2} were adjusted to maintain the appropriate values of DC currents in the windings. Due to the very small supplied voltage levels, the power in both windings was adjusted based on the winding DC resistance and the measured current values (using *A*1, *A*2; see Fig. 1a). In order to keep the power losses at a constant level, the variations of copper resistivity (1) were taken into account:

$$\rho_T = \rho\left[1+\alpha(T-20)\right], \tag{1}$$

where: $\rho = 1.7 \times 10^{-8}\,\Omega$m – copper resistivity at 20°C, ρ_T – copper resistivity at the temperature T, $\alpha = 0{,}004°\text{C}^{-1}$ – temperature coefficient of resistivity.

For each of the described cases, the calibration heating characteristics were recorded. The characteristics presenting the average transformer surface temperatures as a function of time are shown in Fig. 2. It should be noted that the presented calibration method is only valid for these types of transformers. For different electrical components (e.g. different types of transformers, and inductors), the whole procedure must be adjusted.

Based on the curves in Fig. 2, the tested transformer surface temperature increases ΔT_T in the assumed time interval $\Delta t = 5$ minutes were determined. The authors have proposed to measure the temperature transient for max. 15 minutes and then take the temperature difference ΔT_T between 5 and 10 min. In this time interval the transformer temperature rises ΔT_T are approximately a linear time function. During the initial time interval after the start of each calibration test (first 5 minutes of test) the fine adjustment of the applied power is performed.

This made it possible to create the calibration characteristics $P = f(\Delta T_T/\Delta t)$, which are shown in Fig. 3. The characteristics were prepared for the core power losses ("Fe"), the wind-

ings power losses ("2 × Cu") and the core and windings losses ("2 × Cu + Fe") corresponding to three different transformer tests, i.e. no load (predominant core power losses), a short circuit (predominant winding power losses) and a specified load (power losses both in the core and in the windings).

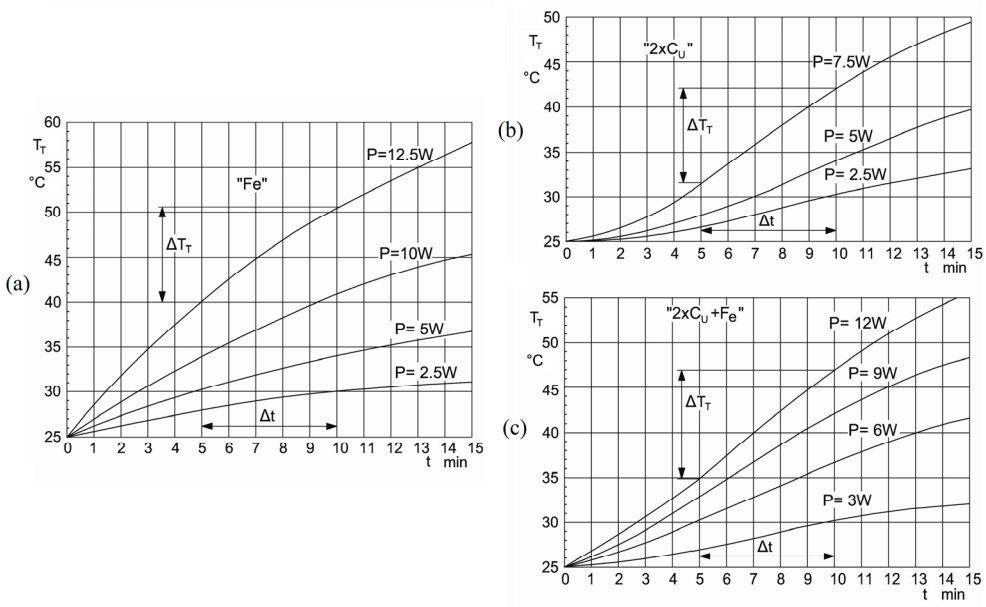

Fig. 2. The heating characteristics of the transformer obtained from the thermal calibration process for different cases (P = const.): (a) power delivered to the core "Fe"; (b) power delivered to the high- and low--voltage windings "2 × Cu"; (c) power delivered to the core and two windings "2 × Cu + Fe"

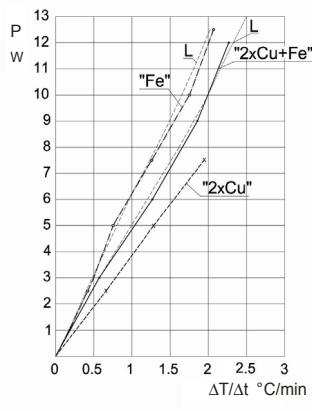

Fig. 3. Calibration characteristics of the transformer $P = f(\Delta T_T/\Delta t)$, where L – linear approximations of the characteristics

2.2. Thermal calibration

AC tests were used as experimental examples, which showed the usefulness of thermal measurements for power loss determination under operating conditions typical of high fre-

quency-transformer applications, i.e. non-sinusoidal voltage and current waveforms. These tests should be performed under thermal conditions identical to those during the calibration process. The same protection case as in the calibration part was used, and during the tests the transformer was placed in the same position as before.

Typically, the waveform shapes of the primary winding current in transformers operating with a rectangular voltage (e.g. transformers in DAB converters) are similar to triangular or trapezoidal ones. A simple way to achieve these conditions with a minimal number of components in the setup is to power supply the tested transformer from an H-bridge converter (Fig. 4). In four cases (no load, short-circuit operation, resistive load operation, and an inductive-load rectifier connected to the secondary winding), the most common typical winding current shapes occured, e.g. the ones corresponding to the current shapes in different operation modes of a DAB converter. In all cases, the high-voltage winding was supplied with an adjustable voltage with a rectangular wave of $f = 100$ kHz.

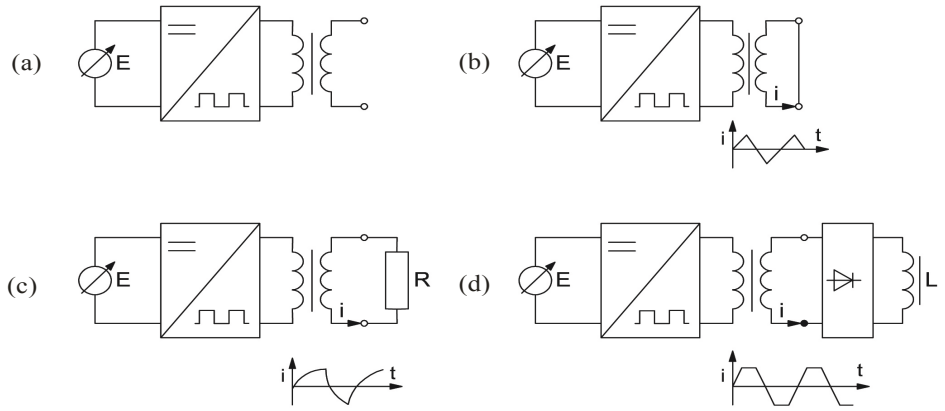

Fig. 4. Representation of the measured systems for different conditions: (a) no load operation; (b) short-circuit operation; (c) resistive load; (d) rectifier with inductive load

During each test, the waveforms of high-voltage winding current with RMS values from 4 A to 12 A and an FFT spectrum of up to the eleventh harmonic were registered (Fig. 5).

For temperature measurements, observations of the transformer surface were carried out using the same thermal camera as in the calibration process. The average values of the surface temperature of the transformer in dynamic thermal states, under the same conditions as in the calibration stage, were registered. In each test, the initial fragments of the heating characteristics were prepared, and for these characteristics, the temperature increments $\Delta T_T = T_{T(t2)} - T_{T(t1)}$ in the time interval from $t_1 = 5$ min to $t_2 = 10$ min were determined.

Based on the derivative $\Delta T_T/\Delta t = (T_{T(t2)} - T_{T(t1)})/(t_2 - t_1)$ determined from the calibration characteristics (given in Fig. 3), the corresponding power losses generated in the transformer were red out.

For determining the power losses in the core of the unloaded transformer, the "Fe" calibration characteristic indicated in Fig. 4 was used. The power losses generated in the transfor-

mer in the short-circuit operation mode (triangular current waveform) were determined based on the calibration characteristics marked as "2×Cu". In this case, it was assumed that due to the low voltage, the power losses in the core could be neglected. For determining the power losses in the transformer with a resistive load (the current waveform being similar to a rectangular one) or with a load in the form of a bridge rectifier (a trapezoidal current waveform), the calibration characteristic "2 × Cu + Fe" was used.

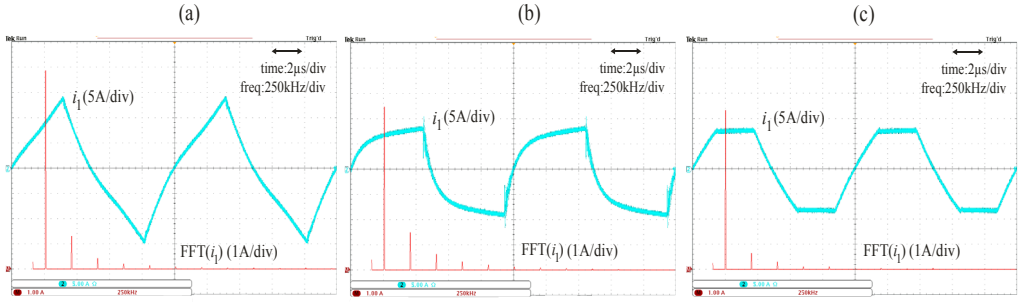

Fig. 5. Waveforms of the current and its spectrums in the high-voltage winding of the transformer in different load conditions: (a) short-circuit ($I_{1(RMS)}$ = 8 A); (b) resistor ($I_{1(RMS)}$ = 6.3 A); (c) bridge rectifier with an inductor in the DC circuit ($I_{1(RMS}$ = 6.7 A)

3. Power loss calculation

3.1. General description of the transformer under testing

A planar transformer as described by the parameters shown in Table 1 was used in all laboratory tests. It was built using two core sets of the ER 64/13/51 type of a typical core material – ferrite 3F3. Multilayer PCBs were used to form the windings of the primary (high-voltage) side, while the windings of the secondary (low-voltage) side were made from copper tape. Both windings were divided into sections to reduce the proximity effect. Based on the geometrical dimensions and construction details of the core and the windings, the DC current resistances of the primary and secondary sides of the transformer windings were calculated and presented in Table 2.

Table 1. Fundamental parameters of the transformer

Parameter	Value
Rated power	S_T = 5600 VA
Maximum primary side voltage (rectangular)	U_1 = 360 V
Windings ratio	$n = N_2/N_1$ = 2/11
Frequency	f = 100 kHz
Max. flux density for U_1 = 360 V, N_1 = 11, f = 100 kHz	B_m = 0.15 T
Effective core volume	V_{Fe} = 52.6 cm^3
Rated current of primary winding	I_1 = 16 A (RMS)
Rated current of secondary winding	I_2 = 88 A (RMS)

Table 2. Main parameters of primary and secondary windings

Parameter	Value
Number of turns (primary)	$N_1 = 11$
Dimensions of a turn (primary)	turn thickness: 0.05 mm average turn width: 18 mm turn length: 0.15 m
Cross-sectional area (primary)	$S_{Cu1} \approx 1.80$ mm^2
Copper filling factor	$k_w = 1.0$
DC current resistance (20°C) of the winding (primary)	$R_{d1} = 15.0$ mΩ
Number of turns (secondary)	$N_2 = 2$
Dimensions of a turn (secondary)	turn thickness: 0.50 mm average turn width: 16 mm turn length: 0.15 m
Cross-sectional area (secondary)	$S_{Cu2} = 32$ mm^2
Copper filling factor (secondary)	$k_w = 1.0$
DC current resistance (20°C) of the windings (secondary)	$R_{d2} = 0.20$ mΩ

3.2. Power losses in the core

For the analytical estimation of the ferrite core losses in the transformer under testing, the following modified Steinmetz equation for rectangular voltages (e.g. [11, 18, 21]) was used:

$$P_{Fe} = \frac{8}{\pi^2} k f^{\alpha} B^{\beta} \left(c_0 + c_1 T_T + c_2 {T_T}^2\right) V_{Fe} \tag{2}$$

where: P_{Fe} is a power losses generated in the core [mW], f, B_m are a frequency and peak value of the flux density, respectively, T_T is a core temperature [°C], c_0, c_1, c_2 are a temperature effect coefficients, V_{Fe} is an effective core volume [cm^3].

The following values for k, α, β and the polynomial coefficients c_0, c_1, and c_2, were assumed (for f=100 kHz) [11]: $k = 0.25\times10^{-3}$; $\alpha = 1.60$; $\beta = 2.50$; $c_0 = 1.26$; $c_1 = 1.05\times10^{-2}$ [°C^{-1}]; $c_2 = 0.79\times10^{-4}$ [°C^{-2}].

It should be noted that the polynomial in formula (2) is only equal to 1 for the core temperatures T_T= 30°C and T_T= 100°C and is minimal (≈ 0.91) for T_T= 65°C.

3.3. Power losses in the windings

In high-frequency operation modes, the skin and proximity effects cause a significant increase in AC resistance and power losses in both windings. A mitigation of the negative impact of these phenomena can be achieved by dividing the winding into sections and alternating the primary and secondary sections.

The resistance of the section j, consisting of m_s layers can be determined using the Dowell's Equation [19, 20]:

$$R_{ac(j)} = R_{d(j)} y \left[\frac{\sinh(2y) + \sin(2y)}{\cosh(2y) - \cos(2y)} + \frac{2}{3}\left({m_s}^2 - 1\right) \frac{\sinh(y) - \sin(y)}{\cosh(y) + \cos(y)} \right] = K_{R(j)} R_{d(j)} \tag{3}$$

where: $R_{d(j)}$ is the resistance of the section j for DC current; $K_{R(j)}$ is the increase rate of the resistance of a winding section for sinusoidal current of the frequency f; m_s is a number of effective layers in the winding section j, y is the relative layer thickness for the copper filling factor equal to 1, expressed as $y = h/\delta$, where δ is the copper skin depth δ determined by the formula

$$\delta = \sqrt{\frac{\rho}{\pi \mu f}} \tag{4}$$

where: μ is a magnetic permeability of copper.

In order to find the AC resistances of the primary R_{ac1} and secondary R_{ac2} windings of a transformer with windings divided into sections, it is necessary to determine the increase rates $K_{R(j)}$ for each section. Next, the coil AC resistance of each section can be calculated: $R_{ac(j)} = K_{R(j)}\, R_{d(j)}$. Finally, by taking into account the series or parallel connection of the sections, the total resistance of the winding is determined.

Fig. 6 shows the cross-section of a high-voltage and low-voltage windings, the corresponding distribution of the magnetic force F_m along the x-axis, and the connection diagram of the windings. It enables the determination of the effective number of sections and layers in the transformer under testing.

In the case of the high-voltage winding, the effective number of layers in the two sections are the same and are equal to $m_{s2} = m_{s4} = 5.5$. The low-voltage winding is divided into three sections: s_1 and s_5 (each of them having two layers $m_{s1} = m_{s5} = 2$), and s_3 (which has four layers, but only two of them are effective, $m_{s3} = 2$).

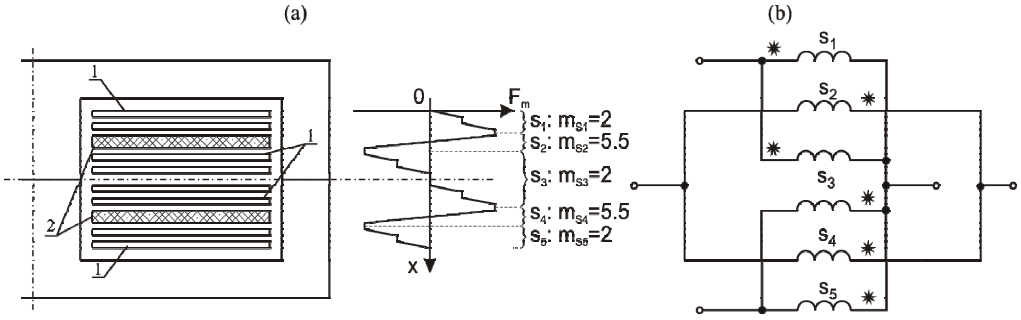

Fig. 6. Windings of the transformer: (a) the configuration of windings in the core window and the distribution of the magnetic force $F_m(x)$: 1 – sections of the low voltage winding, 2 – sections of the high-voltage winding; (b) winding connection diagram

For the winding section with a well-defined effective number of layers and a relative layer thickness y, the coefficient $K_{R(j)} = R_{ac(j)}/R_{d(j)}$ can be taken from Dowell's graphs [19]. When $y \leq 1.5$, (3) can be approximated with a simple expression [23] as below:

$$K_R = 1 + \frac{5m_s^{\,2} - 1}{45} y^4 \tag{5}$$

Equations (3) and (5) as well as Dowell's graphs are only valid for sinusoidal currents. However, the winding currents in the considered transformer are non-sinusoidal. Furthermore, the leakage field produced by the higher harmonic currents penetrates the windings and induces eddy currents which cause an additional increase in the winding resistance. The winding power losses for non-sinusoidal current can be calculated using the RMS values of the effective harmonic currents and the corresponding resistances [11, 24]. The total power losses in the windings are the sum of losses generated by each harmonic current:

$$P_{Cu} = P_{C_{u1}} + P_{C_{u2}} = \sum_{k=1}^{K} {I_{1(k)}}^2 R_{ac1(k)} + \sum_{k=1}^{K} {I_{2(k)}}^2 R_{ac2(k)} \tag{6}$$

where: P_{Cu}, P_{Cu1}, P_{Cu2} are the total power losses generated in the transformer windings and the power losses generated in the high- and low-voltage windings, respectively; $I_{1(k)}$, $I_{2(k)}$ are a RMS harmonic current in the high- and low-voltage windings; $R_{ac1(k)}$, $R_{ac2(k)}$ are resistances of the high- and low-voltage windings for k harmonic currents; K is the order of the harmonic taken into consideration (it is assumed that $K = 11$). The values of $K_{R1(k)}$, $K_{R2(k)}$, $R_{ac1(k)}$ and $R_{ac2(k)}$ are given in Table 3.

Table 3. Resistance increase coefficients and resistances of high- and low-voltage transformer windings for several harmonic currents at 20°C

–	$f_{(1)} = 100$ kHz	$f_{(3)} = 300$ kHz	$f_{(5)} = 500$ kHz	$f_{(7)} = 700$ kHz	$f_{(9)} = 900$ kHz	$f_{(11)} = 1100$ kHz
harmonics No.	$k = 1$	$k = 3$	$k = 5$	$k = 7$	$k = 9$	$k = 11$
$K_{R1(k)}$	1.008	1.0085	1.21	1.40	1.67	1.95
$R_{ac1(k)}$ (mΩ)	15.12	15.127	18.15	21.0	25.05	29.5
$K_{R2(k)}$	7.7	11.5	14.0	18.0	19.5	22.0
$R_{ac2(k)}$ (mΩ)	1.54	2.3	2.8	3.7	3.9	4.4

4. Comparison of the measurements and calculations

The theoretical power losses defined in Section 3 can be directly compared with the measurement results described in Section 2. All calculations were made for the transformer temperature observed during experimental tests ($T_T = 35$°C – the average value of transformer temperature during testing).

The calculations for the transformer without a load were limited to power losses occurring in the core only. The calculations were made using Equation 2 for several U_1 values (from 120 V to 360 V), i.e. identical to those adopted in the experimental part.

The calculations of power dissipated in the windings include the AC current winding resistance, and the values of the measured harmonic current are presented in Table 4. The influence of temperature on the resistivity of the windings material ρ_T (1), the skin depth, and the relative thickness of the layer y were also taken into account [25]. It should be noted that as the temperature increases, the DC resistance of the windings and the skin – depth also increase, reducing the relative thickness of the layer y. In accordance with the (3) and (5) by reducing the value of y the increase coefficient $K_{R(j)} = R_{ac(j)}/R_{dc(j)}$ is also reduced. In the case

of the secondary winding made with copper tape with a thickness $h = 0.5$ mm, at a frequency $f = 100$ kHz, due to the reduction of coefficient $K_{R(j)}$,with increasing temperature the resistance of $R_{ac(2)}$ decreases. For a frequency f =500 kHz, this effect is no longer present (Fig. 7b).

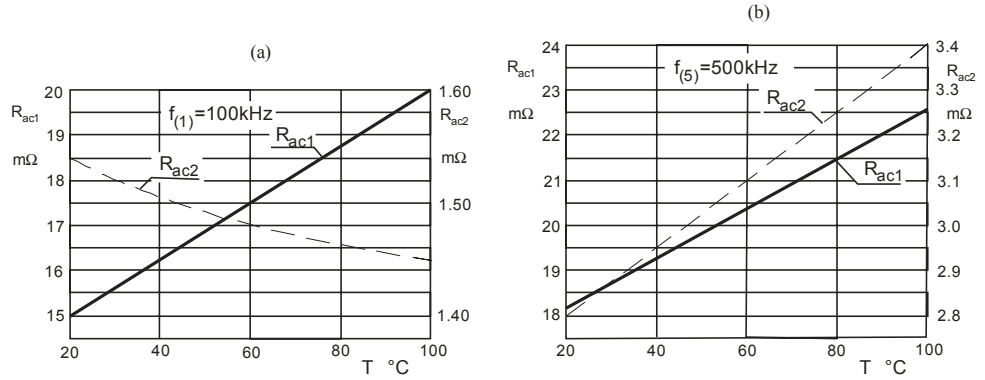

Fig. 7. Resistances of both windings R_{ac1} and R_{ac2} depending on the temperature at frequencies of: (a) $f_{(1)}$ 100 kHz; (b) $f_{(5)}$ = 500 kHz

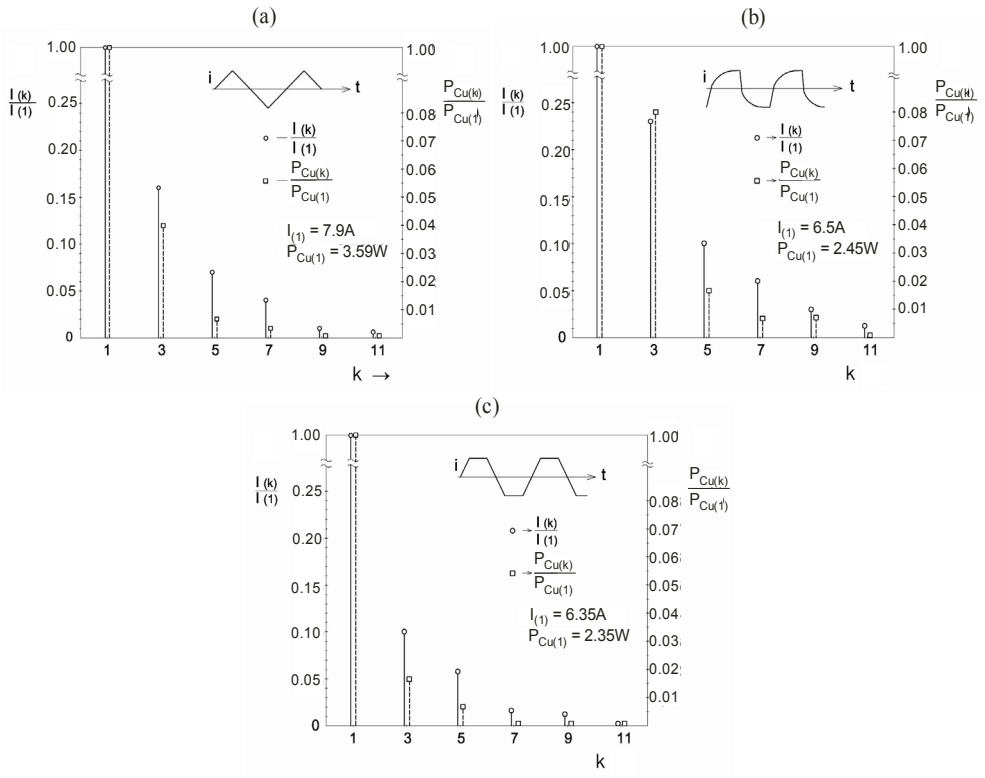

Fig. 8. Relative values of harmonic currents and corresponding power losses in the transformer windings: (a) short-circuit state; (b) transformer with a resistive load; (c) transformer with a rectifier as a load; $I_{(1)}$, $I_{(k)}$ – RMS values of the fundamental and k-th harmonic current components; $P_{Cu(1)}$, $P_{Cu(k)}$ – power losses in both windings caused by the fundamental and k-th harmonic currents

It can be observed that the amplitudes and effective values of the current harmonics of higher order ($k > 1$) are small for the current waveforms occurring in the windings of the transformer supplied with rectangular voltages of 100 kHz (Fig. 5). Therefore, despite the fact that the AC resistances of the windings increased with increasing frequency, the power losses caused by the higher-harmonic currents are relatively low (Fig. 8).

The total power losses in the transformer calculated using (2) and (6) for the core and windings: $P_{cal} = P_{Fe} + P_{Cu}$ are given in Table 4.

Table 4. Transformer power losses as measured using a thermal camera (P_{mea}) and calculated using Steinmetz's and Dowell's formulas (P_{cal}) for the temperature $T_T = 35°C$

Type of load	U_1 **[V]**	I_1 **[A]**	P_{mea} **[W]**	P_{cal} **[W]**	ε_P **[%]**
Δ – short circuit	3.5	4.0	1.10	0.99	10.0
	7.35	8.0	3.70	3.74	–1.10
	10.0	12.0	8.40	8.34	0.70
× – resistor as a load	280	4.0	5.20	5.59	–7.5
	285	5.5	7.0	6.81	2.7
□ – rectifier as a load	18.0	6.37	3.40	3.08	9.4
	25.0	9.13	6.20	5.64	9.0
○ – no load	120.0	0.0	0.58	0.54	6.9
	200.0	0.0	2.33	1.93	17.2
	280.0	0.0	5.10	4.50	11.8
	360.0	0.0	9.25	8.4	9.2

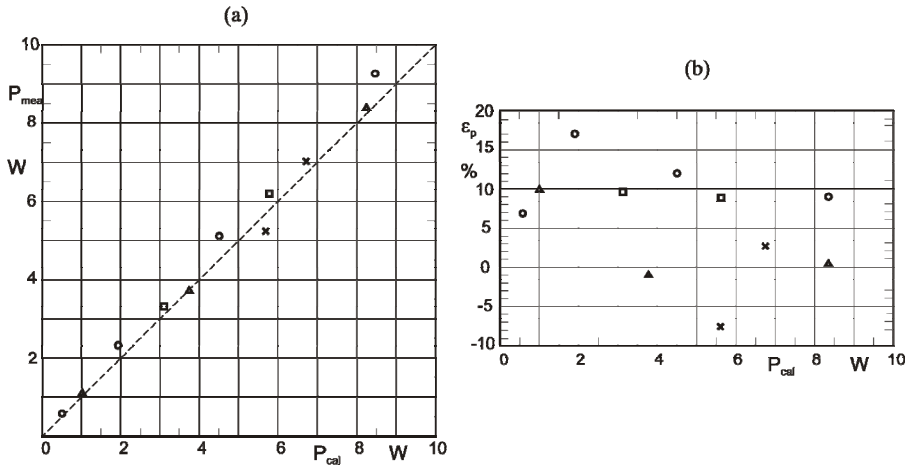

Fig. 9. The absolute (a) and relative (b) difference between the power losses calculated (P_{cal}) and measured using the thermal method (P_{mea}): Δ – short-circuit condition, × – resistive load, □ – rectifier as a load, ○ – no load

In order to provide the comparison of the results for each case, the absolute and the relative differences were calculated (Fig. 9):

$$\varepsilon_R = \frac{P_{mea} - P_{cal}}{P_{mea}} 100\% \tag{7}$$

Due to the fact that the measurements are based on the averaged temperature over a selected area, the accuracy of this method will be better, if the differences between the power dissipated in the windings and in the core are small and the observed surface has a uniform temperature.

5. Conclusions

The growing technical development of thermal cameras enables the quantitative determination of the power losses in electrical components from the thermal images. Moreover, by having high-quality thermal images it is possible to locate the sources of the highest thermal emission.

In this paper, a thermal camera was used to examine the process of heating a planar transformer, while focusing on measuring the power losses occurring in the case of high-frequency voltages and currents. The proposed method is based on determining the temperature rise characteristics of the component being examined, which show the increase of temperature in time based on the known power losses. It is possible to further determine the power losses generated in the element (in various operational conditions) by measuring the increase in temperature over a time interval and comparing it with the result obtained from the calibration process.

The proposed method was described and verified on a planar (5600 VA/100 kHz) transformer using different types of loads which corresponded to the typical operational conditions of a DAB converter. The experimental results have shown good correlation with the analytical calculations made with the use of Steinmetz's and Dowell's equations. The difference between calculated and measured results is in the worst case in the order 10÷20%. This difference originates from the inaccuracy of the thermal imaging method and the analytical calculation.

Furthermore, due to the fact that the increase of temperature in time has been determined in the time interval from five to ten minutes from the start of the test, the presented method is simple and allows high-accuracy measurements to be obtained in a relatively short time. It can be adopted to a wide range of power converters.

The proposed method can also be readily used for determining the power losses in other types of components, such as semiconductor elements.

Acknowledgements

This study was funded by National Science Center Poland in 2010-2013.

References

[1] Xiao C., Chen G., Odendaal W., *Overview of power loss measurement techniques in power electronics systems*, IEEE Transactions on Industrial Application 43(3): 657-664 (2007).

[2] Marinov A., Valchev V., *Improved methodology for power loss measurements in power electronic switches using digital oscilloscope and MATLAB*, Proc. 14th International Power Electronics and Motion Control Conference EPE-PEMC, Ohrid, T7-6-T7-9 (2010).

[3] Feix G., Dieckerhoff S., Allmeling J., Schonberger J., *Simple methods to calculate IGBT and Diode conduction and switching losses*, Proc. European Conf. on Power Electronics and Applications, Barcelona, pp. 1-8 (2009).

[4] Biela J., Badstuebner U., Kolar J.W., *Impact of power density maximization on efficiency DC-DC converter systems*, IEEE Transaction on Power Electronics 24(1): 288-300 (2009).

[5] Pavlovsky M., Hero de Haan S.W., Ferreira J.A., *Reaching high power density in multikilowatt DC-DC converters with galvanic isolation*, IEEE Transaction on Power Electronics 24(3): 603-612 (2009).

[6] Josifović I., Popović-Gerber J., Ferreira J. A., *Power Sandwich Industrial Drive with SiC JFETs*, Proc. 14th European Conference on Power Electronics and Applications *EPE*, Bermingham, pp. 1-10 (2011).

[7] Krismer F., Kolar J.W., *Accurate power loss model derivation of a high-current dual active bridge converter for an automotive application*, IEEE Transactions on Industrial Electronics 57(3): 881-891 (2010).

[8] Krismer F., Kolar J.W., *Closed form solution for minimum conduction loss modulation of DAB converters*, IEEE Transaction on Power Electronics 27(1): 174-188 (2012).

[9] Naayagi R.T., Forsyth A.J., Shuttleworth R., *High-Power bidirectional dc-dc converter for aerospace applications*, IEEE Transaction on Power Electronics 27(11): 2276-2287 (2012).

[10] Li X., Bhat A.K.S., *Analysis and design of high-frequency isolated dual-bridge series resonant dc/dc converter*, IEEE Transaction on Power Electronics 25(4): 850-862 (2010).

[11] Sippola M., Sepponen R.S., *Accurate prediction of high-frequency power transformer losses and temperature rise*, IEEE Transaction on Power Electronics 17(5): 835-847 (2002).

[12] Łyskawiński W., Sujka P., Szeląg W., Barański M., *Numerical analysis of hysteresis loss in pulse transformer*, Archives of Electrical Engineering 60(2): 187-195 (2011).

[13] Stadler A., Gulden C., *Improved thermal design of a high frequency power transformer*, Proc. 14thEuropean Conference on Power Electronics and Applications, EPE, Bermingham, pp. 1-9 (2011).

[14] Conroy D.K., Pierce G.F., Troyk P.R., *Measurement techniques for the design of high-frequency SMPS transformers*, Proc. IEEE 3rd Annual Power Electron. Conf. APOC'88, New Orleans, pp. 341-351 (1988).

[15] Loyau W.V., Bue M.L., Mazaleyrat F., *Measurement of magnetic losses by thermal method applied to power ferrites at high level of induction and frequency*, Review of Scientific Instruments 80(2) (2009).

[16] Kuebrich D., Goettle J., Duerbaum T., *Power Loss Measurement based on Transient Temperature Rise*, IEEE Applied Power Electronics Conference and Exposition, (APEC), Orlando, Florida, USA, 1797-1801 (2012).

[17] Dimitrakakis G.S., Tatakis E.C., Nanakos A.C., *A simple calorimetric setup for the accurate measurement of losses in power electronic converters*, Proc. 14thEuropean Conf. on Power Electronics and Applications, EPE, Bermingham, pp. 1-9 (2011).

[18] Venkatachalam K., Sullivan C.R., Abdallah T., Tacca H., *Accurate prediction of ferrite core loss with nonsinusoidal waveforms using only Steinmetz parameters*, Proc. of IEEE Workshop on Computers in Power Electronics 36-41 (2002).

[19] Dowell P., *Effects of eddy currents in transformer windings*, Proc. IEE 113(8): 1387-1394 (1966).

[20] Pittini R., Zhang Z., Ouyang Z., Andersen M.A.E., Thomson O.C., *Analysis of Planar E+I and ER+I transformers for low-voltage high-current DC/DC converters with focus on winding losses and leakage inductance*, Proc. 7th International Power Electronics and Motion Control Conference ECCE Asia, Harbin, pp. 488-493 (2012).

[21] Villar I., Viscarret U., Etxeberria-Otadui I., Rufer A., *Global loss evaluation methods for non-sinusoidally fed medium-frequency power transformers*, IEEE Transactions on Industrial Electronics 56(10): 4132-4140 (2009).
[22] Nowak M., Grzejszczak P., Zdanowski M., Barlik R., *The thermovision method for the assessment of the winding power losses of a high-frequency planar transformer*, Przegląd Elektrotechniczny (Electrical Review) 88(11): 60-63 (2012).
[23] Hurlley W.G., Wölfe W.H., Breslin J.O., *Opitimized transformer design: inclusive of high-frequency effects*, IEEE Trans. Pow. Electr. 13(4): 651-659 (1998).
[24] Han Y., Eberle W., Liu A., *A practical copper loss measurement method for the planar transformer in high-frequency switching converters*, IEEE Transactions on Industrial Electronics 54(4): 2276-2287 (2007).
[25] Dimitrakakis G.S., Tatakis E.C., *Measurement issues related to high frequency sinusoidal excitation of magnetic coils*, Proc. 35th Annual IEEE Power Electronics Specialists Conference, PESC, Aachen, pp. 1841-1847 (2004).